

1 Gas-particle partitioning of polyol tracers at a suburban site in
2 Nanjing, east China: Increased partitioning to the particle phase

3
4 Chao Qin^a, Yafeng Gou^b, Yuhang Wang^c, Yuhao Mao^b, Hong Liao^b, Qin'geng Wang^d,
5 Mingjie Xie^{b,*}

6
7
8 ^a Colleges of Resources and Environmental Sciences, Nanjing Agricultural University,
9 Nanjing 210095, China

10 ^b Collaborative Innovation Center of Atmospheric Environment and Equipment
11 Technology, Jiangsu Key Laboratory of Atmospheric Environment Monitoring and
12 Pollution Control, School of Environmental Science and Engineering, Nanjing
13 University of Information Science & Technology, 219 Ningliu Road, Nanjing 210044,
14 China

15 ^c School of Earth and Atmospheric Sciences, Georgia Institute of Technology, Atlanta,
16 GA 30332

17 ^d State Key Laboratory of Pollution Control and Resources Reuse, School of the
18 Environment, Nanjing University, Nanjing 210023, China

19
20
21
22 *Corresponding to:

23 Mingjie Xie (mingjie.xie@nuist.edu.cn; mingjie.xie@colorado.edu);

24 Tel: +86-188519037881; Fax: +86-25-58731051;

25 Mailing address: 219 Ningliu Road, Nanjing, Jiangsu, 210044, China

30 **Abstract**

31 Gas-particle partitioning of water-soluble organic compounds plays a significant
32 role in influencing the formation, transport, and lifetime of organic aerosols in the
33 atmosphere, but is poorly characterized. In this work, gas- and particle-phase
34 concentrations of isoprene oxidation products (C5-alkene triols and 2-methylterols),
35 levoglucosan, and sugar polyols were measured simultaneously at a suburban site of
36 the western Yangtze River Delta in east China. All target polyols were primarily
37 distributed into the particle phase (85.9–99.8%). Given the uncertainties in
38 measurements and vapor pressure predictions, a dependence of particle-phase
39 fractions on vapor pressures cannot be determined. To explore the impact of aerosol
40 liquid water on gas-particle partitioning of polyol tracers, three partitioning schemes
41 (*Cases 1-3*) were proposed based on equilibriums of gas versus organic and aqueous
42 phases in aerosols. If particulate organic matter (OM) is presumed as the only
43 absorbing phase (*Case 1*), the measurement-based absorptive partitioning coefficients
44 ($K_{p,OM}^m$) of isoprene oxidation products and levoglucosan were more than 10 times
45 greater than predicted values ($K_{p,OM}^t$). The agreement between $K_{p,OM}^m$ and $K_{p,OM}^t$ was
46 substantially improved when solubility in a separate aqueous phase was included,
47 whenever water-soluble and water-insoluble OM partitioned into separate (*Case 2*) or
48 single (*Case 3*) liquid phases, suggesting that the partitioning of polyol tracers into the
49 aqueous phase in aerosols should not be ignored. The measurement-based effective
50 Henry's law coefficients ($K_{H,e}^m$) of polyol tracers were orders of magnitude higher
51 than their predicted values in pure water ($K_{H,w}^t$). Due to the moderate correlations
52 between $\log(K_{H,e}^m/K_{H,w}^t)$ and molality of sulfate ions, the gap between $K_{H,e}^m$ and
53 $K_{H,w}^t$ of polyol tracers could not be fully parameterized by the equation defining

54 “salting-in” effects, and might be ascribed to mechanisms of reactive uptake, aqueous
55 phase reaction, “like-dissolves-like” principle, etc. These study results also partly
56 reveals the discrepancy between observation and modeling of organic aerosols.

57

58

59

60

61

62

63

64

65

66

67

68

69

70

71

72

73

74

75

76

77 **1 Introduction**

78 The water-soluble organic carbon (WSOC) in ambient aerosols can account for
79 20-80% of particulate organic matter (OM) based on carbon mass (Saxena and
80 Hildemann, 1996; Kondo et al., 2007). Field studies on the hygroscopic growth and
81 cloud condensation nucleus (CCN) activity of aerosol extracts indicated that WSOC
82 contributed significantly to aerosol hygroscopicity, and modified the hydration
83 behavior of inorganic species (e.g., sulfate, nitrate, and ammonium; Hallar et al., 2013;
84 Taylor et al., 2017). Thus, WSOC plays an important role in changing radiative and
85 cloud nucleating properties of atmospheric particles. Particulate WSOC is a complex
86 mixture of polar organic compounds containing oxygenated functional groups (e.g.,
87 hydroxyl, carboxyl, and carbonyl groups), among which a list of organic compounds
88 with multiple hydroxyl (polyols) groups have been identified using gas
89 chromatography -mass spectrometry (GC-MS) and linked with specific emission
90 sources. For example, C5-alkene triols and 2-methyltetrols are isoprene oxidation
91 products (Claeys et al., 2004; Wang et al., 2005; Surratt et al., 2006); levoglucosan is
92 a typical pyrolysis product of cellulose (Simoneit et al., 1999); primary saccharides
93 (e.g., fructose and glucose) and saccharide polyols (e.g., arabitol and mannitol) are
94 commonly associated with soil microbiota and fungal spores, respectively (Simoneit
95 et al., 2004; Bauer et al., 2008).

96 To quantify the sources contributing to WSOC, concentrations of individual
97 organic tracers are often used as inputs for receptor-based modeling (Zhang et al.,
98 2009; Hu et al., 2010). Due to the influences of gas-particle partitioning on source
99 apportionment, Xie et al. (2013, 2014c) suggested the involvement of gas-phase
100 concentrations of organic markers through theoretical prediction or field measurements.

101 The equilibrium absorptive partitioning theory outlined by Pankow (1994a, b) and
102 laboratory measurements of secondary organic aerosol (SOA) yields (Odum et al.,
103 1996) have been widely applied to predict SOA formation in traditional modeling
104 studies (Heald et al., 2005; Volkamer et al., 2006; Hodzic et al., 2010). In addition to
105 absorptive partitioning to particulate OM after the formation of oxygenated organic
106 compounds in gas phase, other formation pathways (e.g., reactive uptake) have been
107 identified and are responsible for the large discrepancy between modeled and
108 observed SOA loadings (Jang et al., 2002; Kroll et al., 2005; Perraud et al., 2012).
109 Unlike non-polar species (e.g., *n*-alkanes, polycyclic aromatic hydrocarbons) and
110 alkanolic acids that are well simulated (Simcik et al., 1998; Xie et al., 2014a; Yatavelli
111 et al., 2014; Isaacman-VanWertz et al., 2016), particle-phase concentrations of
112 carbonyls were underestimated by several orders of magnitude when particulate OM
113 is presumed as the only absorbing phase assuming ideal mixing condition (Healy et al.,
114 2008; Kampf et al., 2013; Shen et al., 2018). Zhao et al. (2013) observed a positive
115 dependence of particle-phase pinonaldehyde on relative humidity (RH, %), and
116 inferred that aerosol water played a role in the formation of pinonaldehyde in the
117 atmosphere. However, very few studies have been performed on the measurement of
118 gaseous polyols (Xie et al., 2014b; Isaacman-VanWertz et al., 2016), and their gas-
119 particle partitioning were poorly understood.

120 Henry's law can describe the uptake of a compound into a liquid, highly dilute
121 solution (e.g., cloud droplets) in the atmosphere (Ip et al., 2009; Compernelle and
122 Müller, 2014a). Aerosol water is also a major component of atmospheric particles,
123 and accounts for 40% by volume at 50% RH in Europe (Tsyro, 2005). But the bulk
124 aerosol solution is highly concentrated with inorganic ions and WSOC. An effective

125 Henry's law coefficient ($K_{H,e}$, mol m⁻³ atm⁻¹) can be used to account for the measured
126 partitioning between the gas phase and aerosol liquid water (Volkamer et al., 2009).
127 Both laboratory and field studies observed enhanced $K_{H,e}$ of carbonyl compounds with
128 inorganic salt concentrations (in mol kg⁻¹ aerosol liquid water content, ALWC; Kampf
129 et al., 2013; Waxman et al., 2015; Shen et al., 2018). This "salting-in" effect
130 (Setschenow, 1889) is not mechanistically understood, and might be linked with the
131 hydrophilic interactions (e.g., hydrogen bonding) between polar organic compounds
132 and inorganic ions leading to an increase of entropy or decrease of Gibbs free energy
133 (Almeida et al., 1983; Waxman et al., 2015). Polyol tracers are highly water-soluble
134 and their gas-particle partitioning is very likely driven by the aqueous phase
135 containing substantial ionic species in ambient aerosols. In the Southeastern US, the
136 particle-phase fraction ($F\%$) of WSOC is highly dependent on RH and ALWC
137 (Hennigan et al., 2009).

138 In the present study, polyols related to specific emission sources in gaseous and
139 particle phases were measured concurrently in northern Nanjing, China. The sampling
140 and chemical analysis were performed in a similar manner as Xie et al. (2014b), while
141 an additional step was added prior to GC-MS analysis to clean the extracts of gaseous
142 samples. To explore the roles of aerosol liquid water on gas-particle partitioning of
143 polyol tracers, three modes (*Cases 1-3*) were proposed based on equilibriums between
144 gas and liquid aerosol phases, and the measurement-based and predicted partitioning
145 coefficients were compared across individual cases. This work tends to explain the
146 gas-particle partitioning of polyols at a suburban site in eastern China, where the
147 estimated average mass concentration of aerosol liquid water is close to 20 $\mu\text{g m}^{-3}$
148 (Yang et al., 2021).

149 **2 Methods**

150 **2.1 Field Sampling**

151 Details of the sampling information were provided in Yang et al. (2021). Briefly,
152 ambient air was sampled on the rooftop of a seven-story library building located in
153 Nanjing University of Information Science and Technology (NUIST 32.21 °N, 118.71
154 °E), a suburban site in the western Yangtze River Delta of east China. A medium
155 volume sampler (PM-PUF-300, Mingye Environmental, Gugangzhou, China)
156 equipped with a 2.5 µm cut impactor was configured to collect particulate matter with
157 aerodynamic diameter less than 2.5 µm (PM_{2.5}) and gaseous organic compounds at a
158 flow rate of 300 L min⁻¹. After the impactor, the sampled air flowed through a filter
159 pack containing two stacked pre-baked (550 °C, 4 h) quartz filters (20.3 cm × 12.6 cm,
160 Munktell Filter AB, Sweden) and a polyurethane foam (PUF, 65 mm diameter × 37.5
161 mm length) cartridge in series. The top quartz filter (Q_f) in the filter pack was loaded
162 with PM_{2.5}; gaseous organic compounds adsorbed on the backup quartz filter (Q_b)
163 were determined to evaluate sampling artifacts; and the PUF cartridge was used for
164 the sampling of gaseous polyols. Filter and PUF samples were collected every sixth
165 day during daytime (8:00 AM – 7:00 PM) and night time (7:00 PM – 7:00 AM next
166 day), respectively, from 09/28/2018 to 09/28/2019. Collection efficiency of gaseous
167 polyols were examined by performing breakthrough experiments using two PUF
168 plugs during nine sampling intervals. Prior to sampling, PUF adsorbents were cleaned
169 and dried in the same way as Xie et al. (2014b). Field blank filter and PUF materials
170 were collected every 10th sample for contamination adjustment. Filter and PUF
171 samples were sealed in prebaked aluminum foil and glass jars, respectively, at – 20 °C
172 until analysis.

173 **2.2 Chemical Analysis**

174 **Bulk speciation.** The accumulated PM_{2.5} mass and bulk components including water
175 soluble ions (NH₄⁺, SO₄²⁻, NO₃⁻, Ca²⁺, Mg²⁺, and K⁺), organic (OC) and elemental
176 carbon (EC), and WSOC were measured for each filter sample. Their final
177 concentrations were determined by subtracting measurement results of Q_b from those
178 of Q_f. Concentrations of aerosol liquid water were predicted by ISORROPIA II model
179 using ambient temperature, RH, and concentration data of NH₄⁺, SO₄²⁻, and NO₃⁻
180 under the metastable state. The estimated water content contributed by hygroscopic
181 WSOC was relatively small (< 1 μg m⁻³) and not accounted for in this work (Text S1
182 of supplementary information). Table S1 lists averages and ranges of ambient
183 temperature, RH, measured PM_{2.5} components, and predicted aerosol liquid water
184 from Yang et al. (2021).

185 **Polyols analysis.** Details of the analysis method for gaseous and particulate polyols
186 were provided in supplementary information (Text S2). Briefly, 1/8 of each filter
187 sample was pre-spiked with deuterated internal standard and extracted ultrasonically
188 twice for 15 min in 10–15 mL of methanol and methylene chloride mixture (1:1, v/v).
189 After filtration, rotary evaporation, N₂ blown down to dryness, and reaction with 50
190 μL of N, O-bis(trimethylsilyl)trifluoroacetamide (BSTFA) containing 1%
191 trimethylchlorosilane (TMCS) and 10 μL of pyridine, the derivatives of polyols were
192 diluted to 400 μL using pure hexane for GC-MS analysis. Pre-spiked PUF samples
193 were Soxhlet extracted using a mixture of 225 mL of methylene chloride and 25 mL
194 of methanol, followed by the same procedures of filter sample pretreatment. Prior to
195 GC-MS analysis, 50 μL of pure water was added to precipitate PUF impurities from
196 the final extract. As shown in Figure S1e, all PUF residues are kept in aqueous phase

197 at the bottom of the vial, while the derivatives of polyol tracers are supposed to be
198 retained in the top clear hexane solution. An aliquot of 2 μL of the supernatant was
199 injected for GC-MS analysis under splitless mode, and an internal standard method
200 with a six-point calibration curve (0.05–5 $\text{ng } \mu\text{L}^{-1}$) was performed to quantify polyols
201 concentrations. In this work, isoprene SOA products, including three C5-alkene triols
202 (cis-2-methyl-1,3,4-trihydroxy-1-butene, 3-methyl-2,3,4-trihydroxy-1-butene, and
203 trans-2-methyl-1,3,4-trihydroxy-1-butene; abbreviated as C5-alkene 1, 2, and 3) and
204 two 2-methyltetrols (2-methylthreitol and 2-methylerythritol), were quantified using
205 meso-erythritol; other polyols were determined using authentic standards.

206 Analytical recoveries of target polyols were obtained by adding known amounts
207 of standards to blank sampling materials (quartz filter and PUF), followed by
208 extraction and instrumental analysis identically as ambient samples. Method detection
209 limits (MDL) of individual species were estimated as three times the standard
210 deviation of their concentrations determined from six injections of the lowest
211 calibration standard. Table S2 lists recovery and MDL values of authentic standard
212 compounds. Concentrations of polyols in field blank samples were measured and
213 subtracted from air samples if necessary. To obtain appropriate gas-particle
214 distribution of polyol tracers, their field-blank corrected concentrations in filter and
215 PUF samples were adjusted by recoveries. Final concentrations of individual polyols
216 in Q_f , Q_b , and PUF samples are summarized in Table S3.

217 **2.3 Data analysis**

218 **Gas-particle separation and breakthrough calculation.** Polyol tracers detected in
219 Q_b samples are contributed by both gaseous adsorption (“positive artifact”) and
220 particle-phase evaporation from Q_f samples (“negative artifact”), but their relative

221 contributions are unknown. Xie et al. (2014b) adjusted particle- and gas-phase
222 concentrations of levoglucosan and 2-methyltetrol based on Q_b measurements in two
223 different ways. One assumed that Q_b values were completely attributed to gaseous
224 adsorption; the other presumed equal contributions from gaseous adsorption and Q_f
225 evaporation. However, negligible difference in gas-particle distribution was observed
226 due to the small Q_b values. In Table S3, concentrations of polyol tracers on Q_b are far
227 below those on Q_f , and it would be safe to presume equal positive and negative
228 artifacts. In this study, particle-phase concentrations of polyols were represented by Q_f
229 values, and the gas phase was calculated as the sum of Q_b and PUF measurements.

230 The sampling efficiency of target polyols were evaluated by collecting and
231 analyzing tandemly installed PUF plugs during nine sampling intervals. The
232 breakthrough of each polyol was calculated as

$$233 \quad B = \frac{[\text{PUF}]_{\text{back}}}{[\text{PUF}]_{\text{front}} + [\text{PUF}]_{\text{backup}}} \times 100\% \quad (1)$$

234 where B is the breakthrough of gaseous sampling, and $[\text{PUF}]$ represents the
235 concentration of specific compound in front or backup PUF sample. A value of 33%
236 was typically used to indicate excessive breakthrough (Peters et al., 2000; Ahrens et
237 al., 2011).

238 **Calculations of partitioning coefficients.** Here, we defined three partitioning cases
239 to explore the influence of dissolution in aerosol liquid water on gas-particle
240 partitioning of polyol tracers in the atmosphere. *Case 1* presumes instantaneous
241 equilibrium between the gas phase and particulate OM based on the equilibrium
242 absorptive partitioning theory. In this case, particulate OM is assumed to be the only
243 absorbing phase and behave as an ideal solution. Then the absorptive gas-particle
244 partitioning coefficients ($K_{p,OM}$, $\text{m}^3 \mu\text{g}^{-1}$) were calculated from measurements ($K_{p,OM}^m$)

245 and predicted theoretically ($K_{p,OM}^t$) as follows (Pankow, 1994a, b; Liang and Pankow,
246 1996; Liang et al., 1997; Mader and Pankow, 2002)

$$247 \quad K_{p,OM}^m = \frac{F/M_{OM}}{A} \quad (2)$$

$$248 \quad K_{p,OM}^t = \frac{RT}{10^6 \overline{MW}_{OM} \zeta_{OM} p_L^\circ} \quad (3)$$

249 where M_{OM} denotes the mass concentration of absorptive organic matter ($OM = OC \times$
250 1.6 ; Turpin and Lim, 2001); F (ng m^{-3}) and A (ng m^{-3}) are particulate and gaseous
251 concentrations of individual polyols, respectively. In eq 3, R ($\text{m}^3 \text{ atm K}^{-1} \text{ mol}^{-1}$) and T
252 (K) are the ideal gas constant and ambient temperature; \overline{MW}_{OM} , average molecular
253 weight of absorptive OM, is set at 200 g mol^{-1} for all samples (Barsanti and Pankow,
254 2004; Williams et al., 2010); ζ_{OM} denotes the mole fraction scale activity coefficient,
255 and is presumed to be unity for all species in each sample; p_L° (atm) is the vapor
256 pressure of each pure compound, and is predicted with several estimation tools and
257 adjusted for each sampling interval based on the average temperature (Text S3 and
258 Table S4).

259 Due to the influence of mixing state and water content in aerosols, several studies
260 modeled the gas-particle partitioning of oxygenated organic compounds by defining a
261 liquid-liquid phase separation (LLPS) in the aerosol (Zuend and Seinfeld, 2012; Pye
262 et al., 2018). The organic-inorganic interactions and changes of activity coefficients in
263 aqueous mixtures were fully considered as well. In this study, we proposed a
264 simplified LLPS partitioning mechanism (*Case 2*) in Figure 1. First, aerosol water and
265 water-insoluble OM ($WIOM = OM - WSOC \times 1.6$) exist in two separate liquid
266 phases, and WSOC and inorganic ions are totally dissolved in the aqueous phase. The
267 distribution of polyol tracers between aqueous (F_w , ng m^{-3}) and WIOM (F_{WIOM} , ng m^{-3})

268 ³) phases is simply depicted by their octanol-water partition coefficients (K_{OW})

$$269 \quad K_{OW} = \frac{F_{WIOM}/V_{WSIOM}}{F_w/V_w} = \frac{c_{WIOM}}{c_w} \quad (4)$$

270 where V_{WIOM} and V_w are volumes (m^3) of WIOM and water in aerosols per cubic
271 meter air; c_{WIOM} and c_w are solution concentrations ($ng\ m^{-3}$) of polyols concentrations
272 in organic and aqueous phases; $\log K_{OW}$ values of target polyols were estimated using
273 the Estimation Programs Interface (EPI) Suite developed by the US Environmental
274 Protection Agency and Syracuse Research Corporation (Table S4; US EPA, 2012).
275 The density of organic matter and water (ρ_w) in aerosols are set at 1.4 and $1.0\ g\ cm^{-3}$,
276 respectively (Isaacman-VanWertz et al., 2016; Taylor et al., 2017). Second, gas-phase
277 polyol tracers are in equilibrium with hydrophobic OM and the aqueous phase,
278 respectively

$$279 \quad K_{p,WIOM}^m = \frac{F_{WIOM}/M_{WIOM}}{A} \quad (5)$$

$$280 \quad K_{H,e}^m = \frac{\frac{F_w}{M_i}}{\frac{A}{M_i} \times R \times T \times \frac{c_{ALW}}{\rho_w}} = \frac{\rho_w \times F_w}{A \times R \times T \times c_{ALW}} \quad (6)$$

281 where $K_{H,e}^m$ ($mol\ m^{-3}\ atm^{-1}$) is the measurement-based effective Henry's law
282 coefficient; M_{WIOM} represents the mass concentration ($\mu g\ m^{-3}$) of WIOM; M_i ($g\ mol^{-1}$)
283 is the molecular weight of specific compound; c_{ALW} ($\mu g\ m^{-3}$) is the mass
284 concentration of aerosol liquid water predicted using ISORROPIA II model. *Case 3* is
285 generally the same as *Case 2*, and the only difference is that water-soluble OM
286 (WSOM) and WIOM exist in a single organic phase. Here total particulate OM was
287 used instead of WIOM to assess the distribution of polyol tracers between aqueous
288 and organic phases, and calculate partitioning coefficients of gas vs. particulate
289 organic ($K_{p,OM}^m$) and aqueous ($K_{H,e}^m$) phases. Note that the polarity of particulate OM
290 phase in *Case 3* was expected to increase, then using K_{OW} to calculate the distribution

291 of polyols between organic and aqueous phases might lead to underestimated $K_{p,OM}^m$
292 and overestimated $K_{H,e}^m$. For comparison purposes, the Henry's law coefficient in
293 pure water at 25 °C ($K_{H,w}^*$) was estimated using EPI and SPARC (Hilal et al., 2008;
294 <http://archemcalc.com/sparc-web/calc>), respectively (Table S4), and was adjusted for
295 each sampling interval due to the changes in ambient temperature using van 't Hoff
296 equation (Text S4).

297 ***Uncertainty estimation.*** To obtain the uncertainty associated with the calculation of $F\%$
298 and partitioning coefficients ($K_{p,OM}^m$ and $K_{H,e}^m$), measurement uncertainties of polyol
299 tracers in filter and PUF samples were estimated from their recoveries and
300 breakthrough for gaseous sampling. The root sum of squares (RSS) method was
301 applied to propagate uncertainties of gas and particle-phase concentrations for $F\%$,
302 $K_{p,OM}^m$, and $K_{H,e}^m$ calculations. Details of the uncertainty estimation and propagation
303 methods were provided in Text S5, and the average relative uncertainties were
304 summarized in Table S5.

305 **3 Results and discussion**

306 ***3.1 Method evaluation***

307 In our previous study, PUF/XAD-4 resin/PUF and PUF/XAD-7 resin/PUF
308 adsorbent sandwiches were tested for sampling gaseous 2-methylterols and
309 levoglucosan (Xie et al., 2014b). The results of breakthrough experiments suggested
310 that both the two sandwiched composites had high sampling efficiency (close to
311 100%). Moreover, individual parts of the two types of composites (top PUF, middle
312 XAD-4/XAD-7 resin, and backup PUF) were analyzed for 7 samples, and target
313 compounds were only detected in top PUF. It is therefore suitable to collect gaseous
314 2-methylterols and levoglucosan using PUF materials only.

315 Although PUF materials were pre-cleaned prior to sampling, a few short-chain
316 polyurethanes or impurities could be dissolved during Soxhlet extraction of target
317 compounds using the mixture of methanol and methylene chloride. These substances
318 precipitated when sample extracts were concentrated (Figure S1a, b), and re-dissolved
319 in BSTFA:TMCS/pyridine and hexane after the derivatization step (Figure S1c, d). In
320 Xie et al. (2014b), an aliquot of 2 μL of the sample extract as shown in Figure S1d
321 was injected for GC-MS analysis. Since the dissolved PUF materials did not vaporize
322 at $\sim 300\text{ }^\circ\text{C}$, the GC inlet liner had to be changed for cleaning every few samples. In
323 this work, 50 μL of pure water was added to separate PUF materials from polyol
324 derivatives in hexane solution. As shown in Figure S1e, all PUF residues were
325 retained in the aqueous solution after phase separation. This pretreatment step was
326 added for the analysis of gaseous samples to save time for changing and cleaning GC
327 inlet liners. However, the revised method did not improve the recoveries of meso-
328 erythritol and levoglucosan in PUF samples (Table S2) compared to those in Xie et al.
329 (2014b). This is because the dissolved PUF materials should have an impact on the
330 derivatization efficiency of polyol species, and future work is warranted to remove
331 dissolved PUF materials in sample extracts before the derivatization step.

332 Measurement results of breakthrough samples and the resulting B values were
333 shown in Figure S2. C5-alkene triols and 2-methyltetrols were mainly observed in
334 summertime, and levoglucosan was only detected in three pairs of breakthrough
335 samples. Their average B values ($< 33\%$) indicated no excessive breakthrough (Figure
336 S2a-c), but were higher than those reported by Xie et al. (2014b). This might be
337 ascribed to the greater face velocity (1.5 cm s^{-1}) for sampling gaseous polyols than
338 that (0.61 cm s^{-1}) in our previous study. Due to the limit in sample number for

339 breakthrough tests and low detection rates, the dependence of breakthrough on
340 ambient temperature or OM loadings cannot be evaluated. The breakthrough of an
341 ideal sampling method is expected to be extremely low (e.g., <10%) and have no
342 dependence on ambient temperature, OM loadings, etc. Unlike fructose which had
343 low breakthrough (Figure S2d), glucose and mannitol had comparable concentrations
344 between front and backup PUF samples for several breakthrough experiments (Figure
345 S2e, f), indicating that PUF materials are not suitable for sampling gaseous glucose
346 and mannitol. Mannose and arabitol were not detected or had BDL values for
347 breakthrough samples, and their breakthrough was not provided. In the current work,
348 concentrations of polyol tracers in filter and PUF samples were all reported, but the
349 data of mannose, glucose, arabitol, and mannitol in PUF samples should be treated
350 with caution due to high breakthrough or the lack of valid breakthrough results.

351 ***3.2 General description of measurement results***

352 Total ambient concentrations ($Q_f + Q_b + \text{PUF}$) of individual polyols are depicted
353 using boxplots in Figure 2. Figure S3 presents temporal variations of total and Q_f
354 concentrations of individual polyols with daytime and night-time measurements
355 distinguished. In general, polyol tracers were predominantly observed on Q_f with
356 averages 1-3 orders of magnitude higher than those on Q_b and PUF (Table S3).
357 Levoglucosan had the highest average total concentration ($66.1 \pm 71.1 \text{ ng m}^{-3}$),
358 followed by fructose ($15.0 \pm 62.9 \text{ ng m}^{-3}$) and mannose ($14.3 \pm 31.3 \text{ ng m}^{-3}$). C5-
359 alkene triols and 2-methyltetrols are formed from isoprene epoxydiols (IEPOX) under
360 low NO_x conditions (Surratt et al., 2010). All the five species on Q_b were more
361 frequently detected and had average concentrations 2-20 times higher than those in
362 PUF samples. While in Xie et al. (2014b), the sum of 2-methyltetrols in Q_b and

363 adsorbent samples were up to 2.7 times higher than those on Q_f in summer Denver, so
364 isoprene products are not similarly distributed between gas and aerosol phases across
365 different regions. Moreover, isoprene-derived polyols exhibited prominent elevations
366 in summer (Figure S3a-e), and their daytime concentrations ($2.02 \pm 3.73 - 10.5 \pm 29.3$
367 ng m^{-3}) were only slightly higher than those during night-time ($1.63 \pm 4.40 - 9.65 \pm$
368 32.7 ng m^{-3}). Previous field studies observed strong diurnal variations of isoprene
369 SOA tracers with peak concentrations from afternoon till midnight (Fu and Kawamura,
370 2011; Isaacman-VanWertz et al., 2016). Although no IEPOX will be generated from
371 the oxidation of isoprene by $\bullet\text{OH}$ and $\text{HO}_2\bullet$ after sunset, the formations of C5-alkene
372 triols and 2-methyltetrols might continue until pre-existing IEPOX is exhausted. In
373 this work, neither the daytime (8:00 AM–7:00 PM) or night-time (7:00 AM–7:00 AM
374 next day) sample covered the whole period when isoprene SOA tracers had peak
375 concentrations, and the strong diurnal variations of C5-alkene triols and 2-
376 methyltetrols were not captured.

377 Levoglucosan was more frequently detected but far less concentrated in PUF than
378 in Q_b samples. Its total concentrations were comparable to those in urban Denver
379 (average $65.3 \pm 96.8 \text{ ng m}^{-3}$, range 2.48 – 478 ng m^{-3}), where an average of ~20%
380 partitioned into the gas phase (Xie et al., 2014b). Due to the enhanced biomass
381 burning activities in cold periods for domestic heating at night, levoglucosan showed
382 a clear seasonal pattern (winter maxima and summer minima) and significant ($p =$
383 0.03) higher concentrations during night-time (Figure S3f). Sugars and sugar alcohols
384 are commonly linked with soil/dust resuspension and associated microbial activities
385 (Simoneit et al., 2004). They were frequently detected in Q_b samples with comparable
386 averages and ranges as those in PUF samples (Table S3). Total concentrations of

387 fructose and glucose were strongly ($r = 0.98$) correlated peaking in middle spring
388 (April 2019, Figure S3h, j), when Ca^{2+} on Q_f also reached its maxima of the year
389 (Yang et al., 2021), indicating an influence from soil/dust resuspension. Arabitol and
390 mannitol had identical seasonal pattern ($r = 0.89$) with elevated total concentrations
391 from May to October (Figure S3i, m), which might be attributed to high levels of
392 vegetation during growing seasons and autumn decomposition (Burshtein et al., 2011).
393 Multiple peaks of mannose concentrations were observed from spring to autumn,
394 suggesting a variety of contributing sources (e.g., microbial activity, vegetation).
395 Xylitol is likely derived from biomass burning in northern Nanjing due to its strong
396 correlation ($r = 0.89$) with levoglucosan.

397 **3.3 Gas- and particle-phase distributions**

398 As mentioned in sections 2.3, concentrations of particulate polyols were obtained
399 directly from Q_f measurements, and the gas phase was calculated as the sum of Q_b and
400 PUF values. Figure S4 shows the time series of gas-phase concentrations and particle-
401 phase fractions ($F\%$) of individual polyol tracers. The average $F\%$ values of measured
402 species are plotted against the logarithms of their liquid-state vapor pressures at 25 °C
403 ($p^{\circ,*}_L$) in Figure 3. Gas-phase C5-alkene triols and 2-methyltetrols had maximum
404 concentrations in summer and significant ($p < 0.05$) day-night variations (Figure S4),
405 while other polyols had extremely low concentrations in the gas phase with $F\%$
406 (average \pm standard deviation) ranging from $94.2 \pm 8.02 - 99.8 \pm 1.21\%$. The average
407 $F\%$ values of 2-methyltetrols ($87.5 \pm 10.6\%$) and levoglucosan ($99.8 \pm 1.21\%$) were
408 greater than those in urban Denver (50–80%; Xie et al., 2014b), where the average
409 sampling temperature (12.5 ± 10.1 °C) was much lower. Thus, the changes in vapor
410 pressures with the ambient temperature and/or particulate OM loadings might not be

411 the main factors driving gas-particle partitioning of polyol tracers in Nanjing. In
412 Figure 3, the average $F\%$ uncertainties (6.16–31.2%) of monosaccharides (e.g.,
413 fructose) and sugar alcohols (e.g., mannitol) were larger than those of isoprene SOA
414 tracers and levoglucosan (3.33–7.24%) due to their low and variable recoveries (Table
415 S2) and excessive breakthrough (Figure S2). However, the estimated uncertainties of
416 $F\%$ for less volatile polyols ($p^{o,*}_L < \sim 10^{-10}$ atm) were not physically meaningful, as
417 more than 95% of these compounds existed in the particle phase. Considering the
418 uncertainties in $F\%$ and $\log p^{o,*}_L$ and high average $F\%$ ($> 85\%$) of target polyol
419 tracers, a dependence of $F\%$ on the vapor pressure could not be determined, and the
420 seasonality and day-night difference ($p > 0.05$) of $F\%$ were obscured.

421 ***3.4 Partitioning coefficients of gas versus organic phases***

422 To understand if particulate OM is the only absorbing phase in aerosols for
423 polyol tracers in Nanjing, the absorptive partitioning coefficients of gas vs. organic
424 phases were calculated based on measurement results ($K^m_{p,OM}$) for predefined *Cases*
425 *1-3* and predicted theoretically ($K^t_{p,OM}$) using eq. 3 and vapor pressures listed in Table
426 S4. In Table 1, $K^t_{p,OM}$ ranges of isoprene SOA tracers, levoglucosan, and meso-
427 erythritol are within two orders of magnitude, while those of monosaccharides and
428 mannitol are larger ($> 10^3$). When particulate OM was assumed as the only absorbing
429 phase (*Case 1*), the average $K^m_{p,OM}$ of isoprene SOA tracers, levoglucosan, and meso-
430 erythritol were more than 10 times greater than most of their $K^t_{p,OM}$ (Table 1), and this
431 difference was not likely susceptible to measurement uncertainties. As shown in Table
432 S5, the average relative uncertainties of measurement-based partitioning coefficients
433 are all $< 50\%$, leading to an uncertainty of $\log K^m_{p,OM}$ less than ± 0.30 . Comparable or
434 even greater (up to 10^5) gap between $K^m_{p,OM}$ and $K^t_{p,OM}$ has been observed for

435 carbonyls in a number of laboratory and field studies (Healy et al., 2008; Zhao et al.,
436 2013; Shen et al., 2018), which could be ascribed to reactive uptake (e.g., hydration,
437 oligomerization, and esterification) of organic gases onto condensed phase (Galloway
438 et al., 2009). Oligomers, sulfate and nitrate esters of 2-methyltetrols can be formed in
439 the aerosol phase (Surratt et al., 2010; Lin et al., 2014), and their decomposition and
440 hydrolysis during filter analysis will lead to an overestimation of particle-phase
441 concentrations (Lin et al., 2013; Cui et al., 2018). However, the occurrence of
442 oligomers, sulfate or nitrate esters of levoglucosan was not ever reported in ambient
443 aerosols, although it can be readily oxidized by $\bullet\text{OH}$ in the aqueous phase of
444 atmospheric particles (Hennigan et al., 2010; Hoffmann et al., 2010).

445 When solubility in aerosol liquid water was considered by assuming a LLPS in
446 ambient aerosols, and whenever WSOM and WIOM partitioned into separate (*Case 2*)
447 or single (*Case 3*) liquid phases, the average $\log K_{\text{p,OM}}^{\text{m}}$ of the above mentioned
448 compounds became much closer to or even lay within the range (e.g., levoglucosan)
449 of $\log K_{\text{p,OM}}^{\text{l}}$ (Table 1). These results indicated that the aerosol liquid water ($21.3 \pm$
450 $24.2 \mu\text{g m}^{-3}$; Table S1) is also an important absorbing phase of ambient polyol tracers
451 in Nanjing. Similarly, the measured average $F\%$ of isoprene SOA tracers in
452 southeastern US and central Amazonia were higher than predictions by assuming
453 instantaneous equilibrium between the gas phase and particulate OM only, and the
454 agreement was improved when parameterization of solubility was included for
455 predictions (Isaacman-VanWertz et al., 2016). But none of these two studies could
456 reasonably predict the temporal variability of $F\%$ or $\log K_{\text{p,OM}}^{\text{m}}$. One possible
457 explanation is that the activity coefficients of isoprene SOA tracers and levoglucosan
458 deviate from unity (0.42–2.04; Pye et al., 2018) and vary with PM composition. Pye

459 et al. (2018) re-analyzed the measurement data from Isaacman-VanWertz et al. (2016)
460 using a thermodynamic equilibrium gas-particle partitioning model in two LLPS
461 modes, which involved organic-inorganic interactions and estimations of activity
462 coefficients as a function of liquid PM mixture composition. The resulting predictions
463 captured both the average and diurnal variations of measured $F\%$ for polyol tracers,
464 suggesting a necessity in obtaining time-resolved activity coefficients for the
465 implementation of absorptive equilibrium partitioning model.

466 Unlike isoprene SOA tracers and levoglucosan, the average $K_{p,OM}^t$ values of
467 monosaccharides (fructose, mannose, and glucose) and sugar alcohols (xylitol,
468 arabitol, and mannitol) were orders of magnitude larger than their $K_{p,OM}^m$ for *Cases 2*
469 *and 3* (Table 1). This is probably caused by the overestimation of gas-phase
470 concentrations of sugar polyols. The organic matter on Q_b is mainly composed of
471 volatile and semi-volatile organic compounds. If the concentrations of organic
472 compounds on Q_b were comparable or higher than those on Q_f , their Q_f values should
473 be dominated by positive artifact. As the vapor pressure decreases, the evaporation
474 loss from Q_f samples becomes non-negligible. Note that the magnitude of negative
475 artifacts is unknown and very difficult to assess, and the vapor pressures of
476 monosaccharides and sugar alcohols are far below 10^{-10} atm (Table S4), their
477 concentrations in Q_b and even PUF samples might contain more contributions from
478 negative artifacts than isoprene SOA tracers and levoglucosan. As low-volatile sugar
479 polyols had lower and less stable recoveries (Table S2) and greater breakthrough
480 (Figure S2e, f), caution is warranted in analyzing their $K_{p,OM}^m$ values obtained in this
481 study.

482 ***3.5 Partitioning coefficients of gas versus aqueous phases***

483 The predicted Henry's law coefficients in pure water ($K_{H,w}^l$, mol m⁻³ atm⁻¹)
484 from EPI and SPARC estimates differed by several orders of magnitude, but literature
485 values of isoprene SOA and levoglucosan were closer to EPI estimates (Table S4). If
486 SPARC $K_{H,w}^{*}$ values were used, the average log $K_{H,e}^m$ of most polyol tracers would be
487 lower than their average log $K_{H,w}^l$ (Table 2), indicating that the aqueous phase of
488 ambient aerosol is less hospitable to polyol tracers than pure water. This is in conflict
489 with the fact that the interactions of organic compounds, water, and inorganic ions in
490 aerosols will increase the partitioning of highly oxygenated compounds (O:C ≥ 0.6;
491 e.g., isoprene SOA tracers and levoglucosan) into the particle phase (Pye et al., 2018).
492 Several studies identified a close relationship between salt concentrations of aerosol
493 water and enhanced uptake of very polar compounds (Almeida et al., 1983; Kroll et
494 al., 2005; Ip et al., 2009; Kampf et al., 2013; Shen et al., 2018). Thus, log $K_{H,w}^l$ values
495 of EPI estimates were used for further data analysis.

496 In Table 2, the $K_{H,w}^l$ values of isoprene SOA tracers, levoglucosan, and meso-
497 erythritols based on EPI estimations were 10² to 10⁶ lower than their corresponding
498 $K_{H,e}^m$. Log $K_{H,e}^m$ values of *Cases 2* and *3* had ignorable difference and were not
499 presented separately. Other polyol compounds exhibited less difference between log
500 $K_{H,e}^m$ and log $K_{H,w}^l$, which was very likely caused by the overestimation of their gas-
501 phase concentrations. The average $K_{H,e}^m$ values of polyol tracers (10¹³–10¹⁵ mol m⁻³
502 atm⁻¹) in this study were several orders of magnitude larger than those of carbonyls
503 derived from ambient measurements (10¹⁰–10¹² mol m⁻³ atm⁻¹; Shen et al., 2018) and
504 chamber simulations (~10¹¹ mol m⁻³ atm⁻¹; Kroll et al., 2005; Volkamer et al., 2006;
505 Galloway et al., 2009). This is because low molecular weight carbonyls (e.g., glyoxal)
506 are much more volatile ($p_L^{0,*} > 10^{-2}$ atm) than our target polyols (Table S4).

507 According to existing studies, the minimum concentrations of gas-phase glyoxal and
508 methylglyoxal in Chinese cities ($\sim 0.1 \mu\text{g m}^{-3}$) are magnitudes higher than the averages
509 of polyol tracers in this work, while their particle-phase concentrations are of the
510 same magnitude (Shen et al., 2018; Liu et al., 2020).

511 A number of previous studies observed enhanced $K_{\text{H,e}}$ of carbonyls with salt
512 concentrations in aqueous solution (Ip et al., 2009; Kampf et al., 2013; Waxman et al.,
513 2015; Shen et al., 2018), and described this “salting-in” effect using

$$514 \text{Log} \left(\frac{K_{\text{H,w}}}{K_{\text{H,e}}} \right) = K_s c_{\text{salt}} \quad (7)$$

515 where K_s (kg mol^{-1}) is the salting constant, and c_{salt} is the aqueous-phase concentration
516 of salt in mol kg^{-1} ALWC. This equation is originally defined in Setschenow (1889)
517 by plotting $\log (K_{\text{H,w}}/K_{\text{H,e}})$ versus the total salt concentration (mol L^{-1}).

518 As sulfate has been identified as the major factor influencing the salting effect of
519 carbonyl species (Kroll et al., 2005; Ip et al., 2009), Figure 4 shows modified
520 Setschenow plots for C5-alkene triols, 2-methyltetrols, and levoglucosan, where \log
521 $(K_{\text{H,w}}^{\text{t}}/K_{\text{H,e}}^{\text{m}})$ values were regressed to the molality of sulfate ion in aerosol liquid
522 water (c_{sulfate} , mol kg^{-1} ALWC). The $\log (K_{\text{H,w}}^{\text{t}}/K_{\text{H,e}}^{\text{m}})$ data increased faster when c_{sulfate}
523 approached 0, and deviated from their expected behavior with increased c_{sulfate} . Kampf
524 et al. (2013) selected a threshold c_{sulfate} of 12 mol kg^{-1} ALWC to illustrate the
525 deviation for chamber experiments, and attributed it to elevated viscosity and slow
526 particle-phase reactions at high c_{sulfate} . In Figure 4, negative correlations ($p < 0.01$) are
527 observed at $c_{\text{sulfate}} < 12 \text{ mol kg}^{-1}$ ALWC, and Figure S5 exhibits significant negative
528 correlations ($p < 0.01$) between $\log (K_{\text{H,w}}^{\text{t}}/K_{\text{H,e}}^{\text{m}})$ and c_{sulfate} for individual polyols even
529 without excluding the deviations at high c_{sulfate} . The K_s values of polyol tracers from
530 Figures 4 and S5 ($-0.17 - -0.037 \text{ kg mol}^{-1}$) are in a similar range as that of glyoxal (-

531 0.24 – -0.04 kg mol⁻¹; Kampf et al., 2013; Shen et al., 2018; Waxman et al., 2015).
532 These results indicated that the shifting of gas-particle equilibrium toward the
533 condensed phase might be partly parameterized by the equation defining “salting-in”
534 effects.

535 However, the “salting-in” effect is a known phenomenon that is not likely linked
536 with a specific physical or chemical mechanism. Quantum chemical calculation
537 results indicated negative Gibbs free energy of water displacement for interactions
538 between SO₄²⁻ and glyoxal monohydrate (Waxman et al., 2015). The net “salting-in”
539 effect of 1-nitro-2-naphthol in NaF solution was interpreted by postulating hydrogen
540 bonding (Almeida et al., 1983). A direct binding of cations to ether oxygens was
541 proposed to be responsible for the increased solubility of water-soluble polymers
542 (Sadeghi and Jahani, 2012). Due to the moderate correlations and negative intercepts
543 in Figures 4 and S5, the gap between $K_{H,e}^l$ and $K_{H,w}^m$ cannot be closed by the “salting-
544 in” effect alone. Shen et al. (2018) also obtained negative intercepts when plotting log
545 ($K_{H,w}^l/K_{H,e}^m$) over c_{sulfate} for glyoxal and methylglyoxal in ambient atmosphere, and
546 attributed this to unknown gas-particle partitioning mechanisms. There is evidence
547 showing that conventional GC/EI-MS analysis overestimates particle-phase 2-
548 methyltetrols by 60-188% due (in part) to the thermal degradation of less volatile
549 oligomers and organosulfates (Cui et al., 2018). To fit the gas-particle distribution of
550 2-methyltetrols in southeastern US, 50% of particulate 2-methyltetrols was presumed
551 to exist in chemical forms with much lower vapor pressures by Pye et al. (2018). So,
552 the reactive uptake and aqueous phase chemistry could be explanations for the
553 enhanced uptake of isoprene SOA tracers. Moreover, log ($K_{H,w}^l/K_{H,e}^m$) values of
554 polyol tracers also negatively correlated with the aqueous-phase concentrations of

555 WSOC (c_{WSOC} , Figure S6), but not NH_4^+ or NO_3^- . This dependence might be
556 associated with the “like-dissolves-like” rule, or indicate the importance of aqueous-
557 phase heterogeneous reactions (Hennigan et al., 2009; Volkamer et al., 2009).
558 Although several studies have estimated Henry’s law constants for a variety of polar
559 organic compounds in pure water (e.g., polyols and polyacids; Compernelle and
560 Müller, 2014a, b), more work is warranted to decrease the estimation uncertainty and
561 explain their increased partitioning toward aerosol liquid water explicitly.

562 **4 Implications and conclusions**

563 In this work, concentrations of gas- and particle-phase polyol tracers were
564 measured simultaneously in northern Nanjing. The temporal variations of individual
565 compounds were dominated by their particle-phase concentrations. Then gas-particle
566 partitioning of polyol tracers should have little influence on source apportionment
567 based on particle-phase data in Nanjing. An improved agreement between
568 measurement-based and predicted $K_{\text{p,OM}}$ of polyol tracers was observed when the
569 solubility in aerosol liquid water was considered, indicating that the aqueous solution
570 in aerosols is also an important absorbing phase. The large gaps of $K_{\text{H,e}}^{\text{m}}$ versus $K_{\text{H,w}}^{\text{t}}$
571 could be partly parameterized using the equation defining “salting-in” effects.
572 According to existing studies, reactive uptake, aqueous phase reactions, and chemical
573 similarity between partitioning species and the absorbing phase might be responsible
574 for increasing the partitioning of polyol tracers into the condensed phase. So, the
575 results of this study have important implications on the prediction of gas-particle
576 partitioning of water-soluble organics, and further studies are required to explain their
577 enhanced aqueous-phase uptake mechanistically. Due to the hygroscopic properties of
578 highly oxidized organic aerosols, this study also partly reveals the discrepancy

579 between modeled and observed SOA in previous studies. However, several
580 assumptions (e.g., LLPS) were made for proposed gas-particle partitioning schemes in
581 this work, more laboratory research is needed to understand the mixing state of
582 inorganic salts, organic components, and aerosol liquid water in atmospheric particles.

583

584 *Data availability*

585 Data used in the writing of this paper is available at the Harvard Dataverse
586 (<https://doi.org/10.7910/DVN/U3IGQR>, Qin et al., 2021)

587

588 *Author contributions*

589 MX designed the research. CQ and YG performed the sampling and chemical analysis.
590 CQ, YM, and MX analyzed the data. CQ and MX wrote the paper with significant
591 contributions from YW, HL, and QW.

592

593 *Competing interests*

594 The authors declare that they have no conflict of interest.

595

596 *Acknowledgements*

597 This research was supported by the National Natural Science Foundation of China
598 (NSFC, 41701551). Y. W. was supported by the National Science Foundation
599 Atmospheric Chemistry Program.

600

601

602

- 604 Ahrens, L., Shoeib, M., Harner, T., Lane, D. A., Guo, R., and Reiner, E. J.: Comparison of annular
605 diffusion denuder and high volume air samplers for measuring per- and polyfluoroalkyl
606 substances in the atmosphere, *Anal. Chem.*, 83, 9622-9628, 10.1021/ac202414w, 2011.
- 607 Almeida, M. B., Alvarez, A. M., Miguel, E. M. D., and Hoyo, E. S. D.: Setchenow coefficients for
608 naphthols by distribution method, *Can. J. Chem.*, 61, 244-248, 10.1139/v83-043, 1983.
- 609 Barsanti, K. C., and Pankow, J. F.: Thermodynamics of the formation of atmospheric organic
610 particulate matter by accretion reactions—Part 1: aldehydes and ketones, *Atmos. Environ.*, 38,
611 4371-4382, 10.1016/j.atmosenv.2004.03.035, 2004.
- 612 Bauer, H., Claeys, M., Vermeylen, R., Schueller, E., Weinke, G., Berger, A., and Puxbaum, H.:
613 Arabitol and mannitol as tracers for the quantification of airborne fungal spores, *Atmos. Environ.*,
614 42, 588-593, <https://doi.org/10.1016/j.atmosenv.2007.10.013>, 2008.
- 615 Burshtein, N., Lang-Yona, N., and Rudich, Y.: Ergosterol, arabitol and mannitol as tracers for biogenic
616 aerosols in the eastern Mediterranean, *Atmos. Chem. Phys.*, 11, 829-839, 10.5194/acp-11-829-
617 2011, 2011.
- 618 Claeys, M., Graham, B., Vas, G., Wang, W., Vermeylen, R., Pashynska, V., Cafmeyer, J., Guyon, P.,
619 Andreae, M. O., Artaxo, P., and Maenhaut, W.: Formation of secondary organic aerosols through
620 photooxidation of isoprene, *Science*, 303, 1173-1176, 10.1126/science.1092805, 2004.
- 621 Compernelle, S., and Müller, J. F.: Henry's law constants of polyols, *Atmos. Chem. Phys.*, 14, 12815-
622 12837, 10.5194/acp-14-12815-2014, 2014a.
- 623 Compernelle, S., and Müller, J. F.: Henry's law constants of diacids and hydroxy polyacids:
624 recommended values, *Atmos. Chem. Phys.*, 14, 2699-2712, 10.5194/acp-14-2699-2014, 2014b.
- 625 Cui, T., Zeng, Z., dos Santos, E. O., Zhang, Z., Chen, Y., Zhang, Y., Rose, C. A., Budisulistiorini, S. H.,
626 Collins, L. B., Bodnar, W. M., de Souza, R. A. F., Martin, S. T., Machado, C. M. D., Turpin, B. J.,
627 Gold, A., Ault, A. P., and Surratt, J. D.: Development of a hydrophilic interaction liquid
628 chromatography (HILIC) method for the chemical characterization of water-soluble isoprene
629 epoxydiol (IEPOX)-derived secondary organic aerosol, *Environmental Science: Environ. Sci.:*
630 *Process. Impacts*, 20, 1524-1536, 10.1039/C8EM00308D, 2018.
- 631 Fu, P., and Kawamura, K.: Diurnal variations of polar organic tracers in summer forest aerosols: A case
632 study of a Quercus and Picea mixed forest in Hokkaido, Japan, *Geochem. J.*, 45, 297-308,
633 10.2343/geochemj.1.0123, 2011.
- 634 Galloway, M. M., Chhabra, P. S., Chan, A. W. H., Surratt, J. D., Flagan, R. C., Seinfeld, J. H., and
635 Keutsch, F. N.: Glyoxal uptake on ammonium sulphate seed aerosol: reaction products and
636 reversibility of uptake under dark and irradiated conditions, *Atmos. Chem. Phys.*, 9, 3331-3345,
637 10.5194/acp-9-3331-2009, 2009.
- 638 Hallar, A. G., Lowenthal, D. H., Clegg, S. L., Samburova, V., Taylor, N., Mazzoleni, L. R., Zielinska,
639 B. K., Kristensen, T. B., Chirokova, G., McCubbin, I. B., Dodson, C., and Collins, D.: Chemical
640 and hygroscopic properties of aerosol organics at Storm Peak Laboratory, *J. Geophys. Res.*
641 *Atmos.*, 118, 4767-4779, <https://doi.org/10.1002/jgrd.50373>, 2013.
- 642 Heald, C. L., Jacob, D. J., Park, R. J., Russell, L. M., Huebert, B. J., Seinfeld, J. H., Liao, H., and
643 Weber, R. J.: A large organic aerosol source in the free troposphere missing from current models,
644 *Geophys. Res. Lett.*, 32, L18809, <https://doi.org/10.1029/2005GL023831>, 2005.
- 645 Healy, R. M., Wenger, J. C., Metzger, A., Duplissy, J., Kalberer, M., and Dommen, J.: Gas/particle
646 partitioning of carbonyls in the photooxidation of isoprene and 1,3,5-trimethylbenzene, *Atmos.*
647 *Chem. Phys.*, 8, 3215-3230, 10.5194/acp-8-3215-2008, 2008.
- 648 Hennigan, C. J., Bergin, M. H., Russell, A. G., Nenes, A., and Weber, R. J.: Gas/particle partitioning of
649 water-soluble organic aerosol in Atlanta, *Atmos. Chem. Phys.*, 9, 3613-3628, 10.5194/acp-9-
650 3613-2009, 2009.
- 651 Hennigan, C. J., Sullivan, A. P., Collett Jr, J. L., and Robinson, A. L.: Levoglucosan stability in
652 biomass burning particles exposed to hydroxyl radicals, *Geophys. Res. Lett.*, 37, L09806,
653 <https://doi.org/10.1029/2010GL043088>, 2010.
- 654 Hilal, S. H., Ayyampalayam, S. N., and Carreira, L. A.: Air-liquid partition coefficient for a diverse set
655 of organic compounds: Henry's Law constant in water and hexadecane, *Environ. Sci. Technol.*,
656 42, 9231-9236, 10.1021/es8005783, 2008.
- 657 Hodzic, A., Jimenez, J. L., Madronich, S., Canagaratna, M. R., DeCarlo, P. F., Kleinman, L., and Fast,
658 J.: Modeling organic aerosols in a megacity: potential contribution of semi-volatile and
659 intermediate volatility primary organic compounds to secondary organic aerosol formation,

660 Atmos. Chem. Phys., 10, 5491-5514, 10.5194/acp-10-5491-2010, 2010.

661 Hoffmann, D., Tilgner, A., Iinuma, Y., and Herrmann, H.: Atmospheric stability of levoglucosan: A
662 detailed laboratory and modeling study, *Environ. Sci. Technol.*, 44, 694-699, 10.1021/es902476f,
663 2010.

664 Hu, D., Bian, Q., Lau, A. K. H., and Yu, J. Z.: Source apportioning of primary and secondary organic
665 carbon in summer PM_{2.5} in Hong Kong using positive matrix factorization of secondary and
666 primary organic tracer data, *J. Geophys. Res. Atmos.*, 115, D16204,
667 <https://doi.org/10.1029/2009JD012498>, 2010.

668 Ip, H. S. S., Huang, X. H. H., and Yu, J. Z.: Effective Henry's law constants of glyoxal, glyoxylic acid,
669 and glycolic acid, *Geophys. Res. Lett.*, 36, L01802, <https://doi.org/10.1029/2008GL036212>, 2009.

670 Isaacman-VanWertz, G., Yee, L. D., Kreisberg, N. M., Wernis, R., Moss, J. A., Hering, S. V., de Sá, S.
671 S., Martin, S. T., Alexander, M. L., Palm, B. B., Hu, W., Campuzano-Jost, P., Day, D. A.,
672 Jimenez, J. L., Riva, M., Surratt, J. D., Viegas, J., Manzi, A., Edgerton, E., Baumann, K., Souza,
673 R., Artaxo, P., and Goldstein, A. H.: Ambient gas-particle partitioning of tracers for biogenic
674 oxidation, *Environ. Sci. Technol.*, 50, 9952-9962, 10.1021/acs.est.6b01674, 2016.

675 Jang, M., Czoschke, N. M., Lee, S., and Kamens, R. M.: Heterogeneous atmospheric aerosol
676 production by acid-catalyzed particle-phase reactions, *Science*, 298, 814,
677 10.1126/science.1075798, 2002.

678 Kampf, C. J., Waxman, E. M., Slowik, J. G., Dommen, J., Pfaffenberger, L., Praplan, A. P., Prévôt, A.
679 S. H., Baltensperger, U., Hoffmann, T., and Volkamer, R.: Effective Henry's law partitioning and
680 the salting constant of glyoxal in aerosols containing sulfate, *Environ. Sci. Technol.*, 47, 4236-
681 4244, 10.1021/es400083d, 2013.

682 Kondo, Y., Miyazaki, Y., Takegawa, N., Miyakawa, T., Weber, R. J., Jimenez, J. L., Zhang, Q., and
683 Worsnop, D. R.: Oxygenated and water-soluble organic aerosols in Tokyo, *J. Geophys. Res.*
684 *Atmos.*, 112, D01203, 10.1029/2006jd007056, 2007.

685 Kroll, J. H., Ng, N. L., Murphy, S. M., Varutbangkul, V., Flagan, R. C., and Seinfeld, J. H.: Chamber
686 studies of secondary organic aerosol growth by reactive uptake of simple carbonyl compounds, *J.*
687 *Geophys. Res. Atmos.*, 110, D23207, <https://doi.org/10.1029/2005JD006004>, 2005.

688 Liang, C., and Pankow, J. F.: Gas/particle partitioning of organic compounds to environmental tobacco
689 smoke: Partition coefficient measurements by desorption and comparison to urban particulate
690 material, *Environ. Sci. Technol.*, 30, 2800-2805, 10.1021/es960050x, 1996.

691 Liang, C., Pankow, J. F., Odum, J. R., and Seinfeld, J. H.: Gas/particle partitioning of semivolatile
692 organic compounds to model inorganic, organic, and ambient smog aerosols, *Environ. Sci.*
693 *Technol.*, 31, 3086-3092, 10.1021/es9702529, 1997.

694 Lin, Y.-H., Budisulistiorini, S. H., Chu, K., Siejack, R. A., Zhang, H., Riva, M., Zhang, Z., Gold, A.,
695 Kautzman, K. E., and Surratt, J. D.: Light-absorbing oligomer formation in secondary organic
696 aerosol from reactive uptake of isoprene epoxydiols, *Environ. Sci. Technol.*, 48, 12012-12021,
697 10.1021/es503142b, 2014.

698 Lin, Y. H., Knipping, E. M., Edgerton, E. S., Shaw, S. L., and Surratt, J. D.: Investigating the
699 influences of SO₂ and NH₃ levels on isoprene-derived secondary organic aerosol formation using
700 conditional sampling approaches, *Atmos. Chem. Phys.*, 13, 8457-8470, 10.5194/acp-13-8457-
701 2013, 2013.

702 Liu, J., Li, X., Li, D., Xu, R., Gao, Y., Chen, S., Liu, Y., Zhao, G., Wang, H., Wang, H., Lou, S., Chen,
703 M., Hu, J., Lu, K., Wu, Z., Hu, M., Zeng, L., and Zhang, Y.: Observations of glyoxal and
704 methylglyoxal in a suburban area of the Yangtze River Delta, China, *Atmos. Environ.*, 238,
705 117727, <https://doi.org/10.1016/j.atmosenv.2020.117727>, 2020.

706 Mader, B. T., and Pankow, J. F.: Study of the effects of particle-phase carbon on the gas/particle
707 partitioning of semivolatile organic compounds in the atmosphere using controlled field
708 experiments, *Environ. Sci. Technol.*, 36, 5218-5228, 10.1021/es011048v, 2002.

709 Odum, J. R., Hoffmann, T., Bowman, F., Collins, D., Flagan, R. C., and Seinfeld, J. H.: Gas/particle
710 partitioning and secondary organic aerosol yields, *Environ. Sci. Technol.*, 30, 2580-2585,
711 10.1021/es950943+, 1996.

712 Pankow, J. F.: An absorption model of the gas/aerosol partitioning involved in the formation of
713 secondary organic aerosol, *Atmos. Environ.*, 28, 189-193, 10.1016/1352-2310(94)90094-9, 1994a.

714 Pankow, J. F.: An absorption model of gas/particle partitioning of organic compounds in the
715 atmosphere, *Atmos. Environ.*, 28, 185-188, 10.1016/1352-2310(94)90093-0, 1994b.

716 Perraud, V., Bruns, E. A., Ezell, M. J., Johnson, S. N., Yu, Y., Alexander, M. L., Zelenyuk, A., Imre,
717 D., Chang, W. L., Dabdub, D., Pankow, J. F., and Finlayson-Pitts, B. J.: Nonequilibrium

718 atmospheric secondary organic aerosol formation and growth, *Proc. Natl. Acad. Sci. U.S.A.*, 109,
719 2836-2841, 10.1073/pnas.1119909109, 2012.

720 Peters, A. J., Lane, D. A., Gundel, L. A., Northcott, G. L., and Jones, K. C.: A comparison of high
721 volume and diffusion denuder samplers for measuring semivolatile organic compounds in the
722 atmosphere, *Environ. Sci. Technol.*, 34, 5001-5006, 10.1021/es000056t, 2000.

723 Pye, H. O. T., Zuend, A., Fry, J. L., Isaacman-VanWertz, G., Capps, S. L., Appel, K. W., Foroutan, H.,
724 Xu, L., Ng, N. L., and Goldstein, A. H.: Coupling of organic and inorganic aerosol systems and
725 the effect on gas-particle partitioning in the southeastern US, *Atmos. Chem. Phys.*, 18, 357-370,
726 10.5194/acp-18-357-2018, 2018.

727 Qin, C., Gou, Y., Wang, Y., Mao, Y., Liao, H., Wang, Q. g., and Xie, M.: Replication Data for: Gas-
728 particle partitioning of polyol tracers in the western Yangtze River Delta, China, in, VI ed.,
729 Harvard Dataverse, <https://doi.org/10.7910/DVN/U3IGQR>, 2021.

730 Sadeghi, R., and Jahani, F.: Salting-in and salting-out of water-soluble polymers in aqueous salt
731 solutions, *J. Phys. Chem. B*, 116, 5234-5241, 10.1021/jp300665b, 2012.

732 Saxena, P., and Hildemann, L.: Water-soluble organics in atmospheric particles: A critical review of
733 the literature and application of thermodynamics to identify candidate compounds, *J. Atmos.*
734 *Chem.*, 24, 57-109, 10.1007/bf00053823, 1996.

735 Setschenow, J.: Über die Konstitution der Salzlösungen auf Grund ihres Verhaltens zu Kohlensäure, *Z.*
736 *Phys. Chem.*, 4U, 117-125, <https://doi.org/10.1515/zpch-1889-0409>, 1889.

737 Shen, H., Chen, Z., Li, H., Qian, X., Qin, X., and Shi, W.: Gas-particle partitioning of carbonyl
738 compounds in the ambient atmosphere, *Environ. Sci. Technol.*, 52, 10997-11006,
739 10.1021/acs.est.8b01882, 2018.

740 Simcik, M. F., Franz, T. P., Zhang, H., and Eisenreich, S. J.: Gas-particle partitioning of PCBs and
741 PAHs in the Chicago urban and adjacent coastal atmosphere: States of equilibrium, *Environ. Sci.*
742 *Technol.*, 32, 251-257, 10.1021/es970557n, 1998.

743 Simoneit, B. R. T., Schauer, J. J., Nolte, C. G., Oros, D. R., Elias, V. O., Fraser, M. P., Rogge, W. F.,
744 and Cass, G. R.: Levoglucosan, a tracer for cellulose in biomass burning and atmospheric
745 particles, *Atmos. Environ.*, 33, 173-182, [http://dx.doi.org/10.1016/S1352-2310\(98\)00145-9](http://dx.doi.org/10.1016/S1352-2310(98)00145-9), 1999.

746 Simoneit, B. R. T., Elias, V. O., Kobayashi, M., Kawamura, K., Rushdi, A. I., Medeiros, P. M., Rogge,
747 W. F., and Didyk, B. M.: Sugars dominant water-soluble organic compounds in soils and
748 characterization as tracers in atmospheric particulate matter, *Environ. Sci. Technol.*, 38, 5939-
749 5949, 10.1021/es0403099, 2004.

750 Surratt, J. D., Murphy, S. M., Kroll, J. H., Ng, N. L., Hildebrandt, L., Sorooshian, A., Szmigielski, R.,
751 Vermeylen, R., Maenhaut, W., Claeys, M., Flagan, R. C., and Seinfeld, J. H.: Chemical
752 composition of secondary organic aerosol formed from the photooxidation of isoprene, *J. Phys.*
753 *Chem. A*, 110, 9665-9690, 10.1021/jp061734m, 2006.

754 Surratt, J. D., Chan, A. W. H., Eddingsaas, N. C., Chan, M., Loza, C. L., Kwan, A. J., Hersey, S. P.,
755 Flagan, R. C., Wennberg, P. O., and Seinfeld, J. H.: Reactive intermediates revealed in secondary
756 organic aerosol formation from isoprene, *Proc. Natl. Acad. Sci. U.S.A.*, 107, 6640-6645,
757 10.1073/pnas.0911114107, 2010.

758 Taylor, N. F., Collins, D. R., Lowenthal, D. H., McCubbin, I. B., Hallar, A. G., Samburova, V.,
759 Zielinska, B., Kumar, N., and Mazzoleni, L. R.: Hygroscopic growth of water soluble organic
760 carbon isolated from atmospheric aerosol collected at US national parks and Storm Peak
761 Laboratory, *Atmos. Chem. Phys.*, 17, 2555-2571, 10.5194/acp-17-2555-2017, 2017.

762 Tsyro, S. G.: To what extent can aerosol water explain the discrepancy between model calculated and
763 gravimetric PM10 and PM2.5?, *Atmos. Chem. Phys.*, 5, 515-532, 10.5194/acp-5-515-2005, 2005.

764 Turpin, B. J., and Lim, H.-J.: Species contributions to PM2.5 mass concentrations: Revisiting common
765 assumptions for estimating organic mass, *Aerosol Sci. Technol.*, 35, 602-610,
766 10.1080/02786820119445, 2001.

767 US EPA: Estimation Program Interface (EPI) Suite. Version v4.11, 2012. United States Environmental
768 Protection Agency, Washington, DC, USA. [https://www.epa.gov/tsca-screening-tools/download-](https://www.epa.gov/tsca-screening-tools/download-epi-suite-estimation-program-interface-v411)
769 [epi-suite-estimation-program-interface-v411](https://www.epa.gov/tsca-screening-tools/download-epi-suite-estimation-program-interface-v411)

770 Volkamer, R., Jimenez, J. L., San Martini, F., Dzepina, K., Zhang, Q., Salcedo, D., Molina, L. T.,
771 Worsnop, D. R., and Molina, M. J.: Secondary organic aerosol formation from anthropogenic air
772 pollution: Rapid and higher than expected, *Geophys. Res. Lett.*, 33, L17811,
773 <https://doi.org/10.1029/2006GL026899>, 2006.

774 Volkamer, R., Ziemann, P. J., and Molina, M. J.: Secondary Organic Aerosol Formation from
775 Acetylene (C2H2): seed effect on SOA yields due to organic photochemistry in the aerosol

776 aqueous phase, *Atmos. Chem. Phys.*, 9, 1907-1928, 10.5194/acp-9-1907-2009, 2009.

777 Wang, W., Kourtchev, I., Graham, B., Cafmeyer, J., Maenhaut, W., and Claeys, M.: Characterization
778 of oxygenated derivatives of isoprene related to 2-methyltetrols in Amazonian aerosols using
779 trimethylsilylation and gas chromatography/ion trap mass spectrometry, *Rapid Commun. Mass*
780 *Spectrom.*, 19, 1343-1351, <https://doi.org/10.1002/rcm.1940>, 2005.

781 Waxman, E. M., Elm, J., Kurtén, T., Mikkelsen, K. V., Ziemann, P. J., and Volkamer, R.: Glyoxal and
782 methylglyoxal Setschenow salting constants in sulfate, nitrate, and chloride solutions:
783 Measurements and Gibbs energies, *Environ. Sci. Technol.*, 49, 11500-11508,
784 10.1021/acs.est.5b02782, 2015.

785 Williams, B. J., Goldstein, A. H., Kreisberg, N. M., and Hering, S. V.: In situ measurements of
786 gas/particle-phase transitions for atmospheric semivolatile organic compounds, *Proc. Natl. Acad.*
787 *Sci. U.S.A.*, 107, 6676-6681, 10.1073/pnas.0911858107, 2010.

788 Xie, M., Barsanti, K. C., Hannigan, M. P., Dutton, S. J., and Vedal, S.: Positive matrix factorization of
789 PM_{2.5} - eliminating the effects of gas/particle partitioning of semivolatile organic compounds,
790 *Atmos. Chem. Phys.*, 13, 7381-7393, 10.5194/acp-13-7381-2013, 2013.

791 Xie, M., Hannigan, M. P., and Barsanti, K. C.: Gas/particle partitioning of n-alkanes, PAHs and
792 oxygenated PAHs in urban Denver, *Atmos. Environ.*, 95, 355-362,
793 <http://dx.doi.org/10.1016/j.atmosenv.2014.06.056>, 2014a.

794 Xie, M., Hannigan, M. P., and Barsanti, K. C.: Gas/particle partitioning of 2-methyltetrols and
795 levoglucosan at an urban site in Denver, *Environ. Sci. Technol.*, 48, 2835-2842,
796 10.1021/es405356n, 2014b.

797 Xie, M., Hannigan, M. P., and Barsanti, K. C.: Impact of gas/particle partitioning of semivolatile
798 organic compounds on source apportionment with positive matrix factorization, *Environ. Sci.*
799 *Technol.*, 48, 9053-9060, 10.1021/es5022262, 2014c.

800 Yang, L., Shang, Y., Hannigan, M. P., Zhu, R., Wang, Q. g., Qin, C., and Xie, M.: Collocated
801 speciation of PM_{2.5} using tandem quartz filters in northern nanjing, China: Sampling artifacts and
802 measurement uncertainty, *Atmos. Environ.*, 246, 118066,
803 <https://doi.org/10.1016/j.atmosenv.2020.118066>, 2021.

804 Yatavelli, R. L. N., Stark, H., Thompson, S. L., Kimmel, J. R., Cubison, M. J., Day, D. A.,
805 Campuzano-Jost, P., Palm, B. B., Hodzic, A., Thornton, J. A., Jayne, J. T., Worsnop, D. R., and
806 Jimenez, J. L.: Semicontinuous measurements of gas-particle partitioning of organic acids in a
807 ponderosa pine forest using a MOVI-HRTof-CIMS, *Atmos. Chem. Phys.*, 14, 1527-1546,
808 10.5194/acp-14-1527-2014, 2014.

809 Zhang, Y., Sheesley, R. J., Schauer, J. J., Lewandowski, M., Jaoui, M., Offenber, J. H., Kleindienst, T.
810 E., and Edney, E. O.: Source apportionment of primary and secondary organic aerosols using
811 positive matrix factorization (PMF) of molecular markers, *Atmos. Environ.*, 43, 5567-5574,
812 <https://doi.org/10.1016/j.atmosenv.2009.02.047>, 2009.

813 Zhao, Y., Kreisberg, N. M., Worton, D. R., Isaacman, G., Weber, R. J., Liu, S., Day, D. A., Russell, L.
814 M., Markovic, M. Z., VandenBoer, T. C., Murphy, J. G., Hering, S. V., and Goldstein, A. H.:
815 Insights into secondary organic aerosol formation mechanisms from measured gas/particle
816 partitioning of specific organic tracer compounds, *Environ. Sci. Technol.*, 47, 3781-3787,
817 10.1021/es304587x, 2013.

818 Zuend, A., and Seinfeld, J. H.: Modeling the gas-particle partitioning of secondary organic aerosol: the
819 importance of liquid-liquid phase separation, *Atmos. Chem. Phys.*, 12, 3857-3882, 10.5194/acp-
820 12-3857-2012, 2012.

821

Table 1. Comparisons of measurement-based $\log K_{p,OM}$ ($\text{m}^3 \mu\text{g}^{-1}$) at three proposed cases and predicted values.

Species	No. of obs.	Log $K_{p,OM}^m$ ^a			Log $K_{p,OM}^b$			
		Case 1	Case 2	Case 3	EPI	EVAPORATION	SPARC	SIMPOL
Isoprene SOA tracers								
C5-alkene triol 1	53	0.33 ± 0.71	-0.79 ± 0.86	-0.82 ± 0.85	-3.09	-2.84	-1.19	-2.88
C5-alkene triol 2	63	0.15 ± 0.55	-1.02 ± 0.74	-1.05 ± 0.73	-3.62	-3.67	-4.14	-2.85
C5-alkene triol 3	83	0.35 ± 0.68	-0.83 ± 0.86	-0.86 ± 0.85	-2.90	-2.65	-1.00	-2.69
2-Methylthreitol	101	-0.12 ± 0.48	-2.09 ± 0.71	-2.09 ± 0.70	-1.87	-1.30	-1.18	-0.47
2-Methylerythritol	95	-0.011 ± 0.58	-1.96 ± 0.71	-1.96 ± 0.71	-1.90	-1.34	-1.22	-0.50
Biomass burning tracer								
Levogluconan	65	2.23 ± 0.72	0.63 ± 0.90	0.62 ± 0.90	-0.04	-0.81	1.04	-0.76
Sugars and sugar alcohols								
Meso-erythritol	31	0.87 ± 0.53	-1.43 ± 0.60	-1.43 ± 0.60	-0.65	-1.21	-0.45	
Fructose	85	0.65 ± 0.73	-1.20 ± 0.83	-1.20 ± 0.89	1.17	2.76	6.94	
Mannose	74	0.62 ± 0.71	-2.12 ± 0.95	-2.12 ± 0.95	1.28	2.13	4.77	
Glucose	88	0.42 ± 0.67	-2.77 ± 0.93	-2.77 ± 0.93	0.34	3.75	7.32	
Xylitol	22	0.24 ± 0.54	-2.61 ± 0.72	-2.61 ± 0.72	3.37	2.34	3.57	
Arabitol	30	1.46 ± 0.89	-1.35 ± 1.24	-1.35 ± 1.24	3.25	1.67	2.90	
Manitol	65	1.08 ± 0.63	-2.24 ± 0.95	-2.24 ± 0.95	2.33	4.16	6.68	

^a Logarithms with base 10, average ± standard deviation; ^b temperature range: -4–36 °C.

Table 2. Comparisons of measurement-based $\log K_{H,e}$ ($\text{mol m}^{-3} \text{atm}^{-1}$) and predicted $\log K_{H,w}$ of individual polyol tracers.

Species	No. of obs.	Log $K_{H,e}^m$ (Cases 2) ^a			Log $K_{H,w}^t$ ^b	
		Median	Average	Range	EPI	SPARC
<i>Isoprene SOA tracers</i>						
C5-alkene triol 1	53	14.0	13.9 ± 0.86	11.5 – 16.4	7.22	11.7
C5-alkene triol 2	63	13.7	13.6 ± 0.73	11.2 – 16.1	7.34	7.66
C5-alkene triol 3	83	13.9	13.8 ± 0.85	10.6 – 16.1	7.43	11.9
2-Methylthreitol	101	13.4	13.3 ± 0.70	10.9 – 14.8	10.0	14.1
2-Methylerythritol	95	13.5	13.5 ± 0.71	11.6 – 15.6	9.95	14.1
<i>Biomass burning tracer</i>						
Levoglucozan	65	15.7	15.7 ± 0.90	13.2 – 17.3	13.4	16.1
<i>Sugars and sugar alcohols</i>						
Meso-erythritol	31	14.5	14.4 ± 0.60	12.8 – 15.6	9.65	13.8
Fructose	85	14.2	14.1 ± 0.89	11.9 – 16.5	14.7	19.9
Mannose	74	14.0	14.1 ± 0.94	12.1 – 16.8	10.9	18.8
Glucose	88	13.9	13.9 ± 0.93	11.3 – 16.3	14.7	20.9
Xylitol	22	13.8	13.7 ± 0.72	12.6 – 15.0	12.1	18.1
Arabitol	30	15.1	15.0 ± 1.23	13.0 – 18.2	11.3	17.4
Mannitol	65	14.6	14.5 ± 0.94	12.1 – 16.4	12.9	20.8

^a Logarithms with base 10 ($\log K_{H,e}^m$ values of Case 3 had ignorable difference, and were not exhibited separately); ^b temperature range: -4~36 °C.

Figure 1

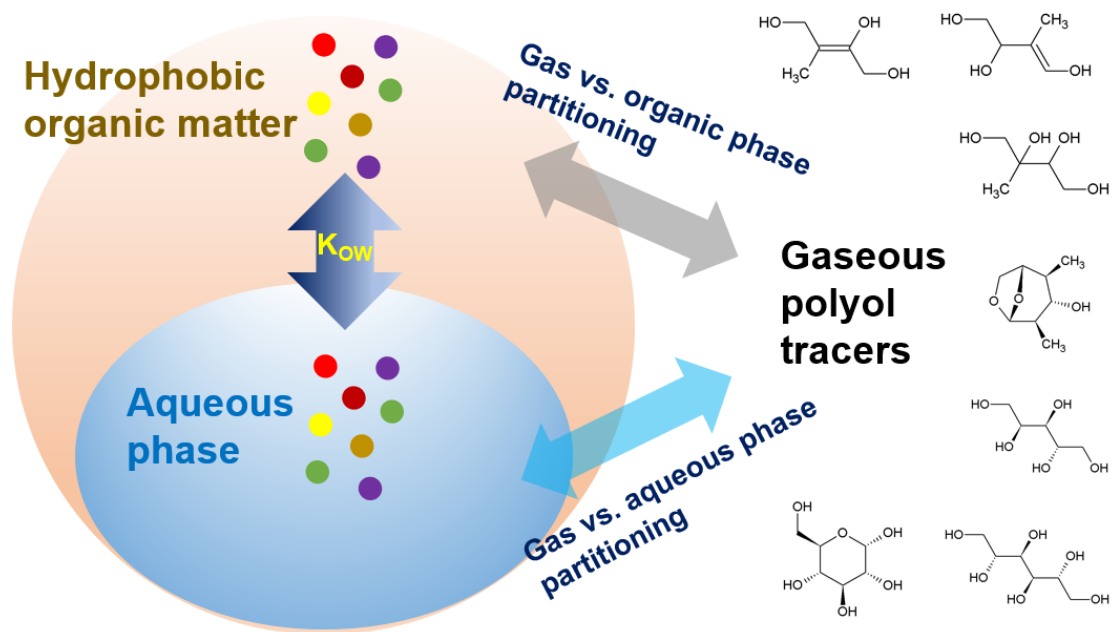


Figure 1. Proposed scheme for gas-particle partitioning of polyol tracers.

Figure 2

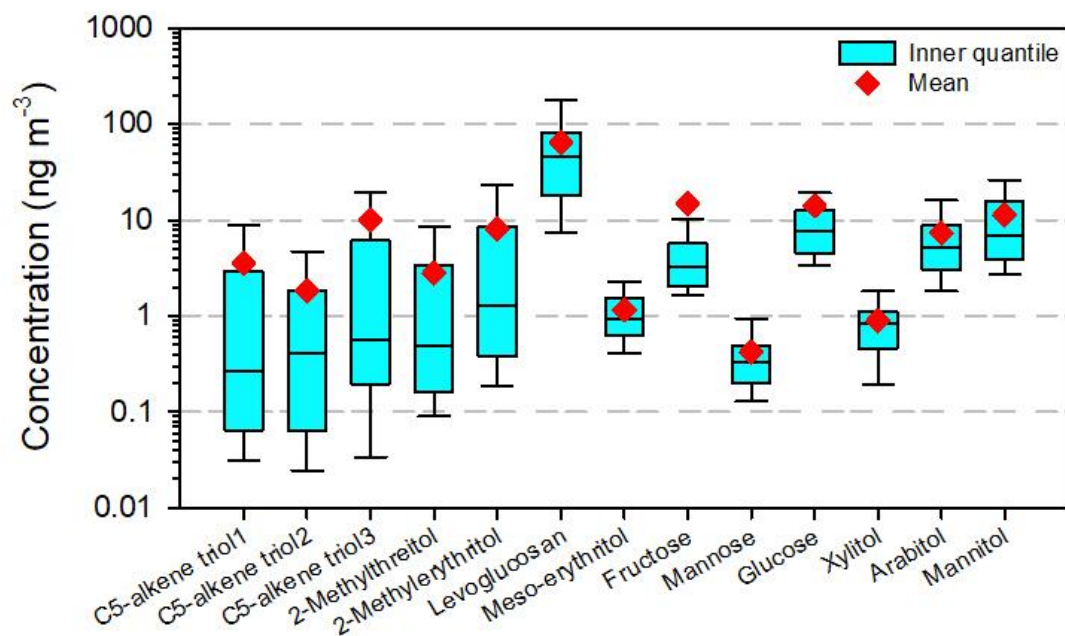


Figure 2. Total concentrations of individual polyols ($Q_f + Q_b + \text{PUF}$) in the ambient atmosphere of northern Nanjing. The boxes depict the median (dark line), inner quantile range (box), 10th and 90th percentiles (whiskers), and the mean (red diamond).

Figure 3

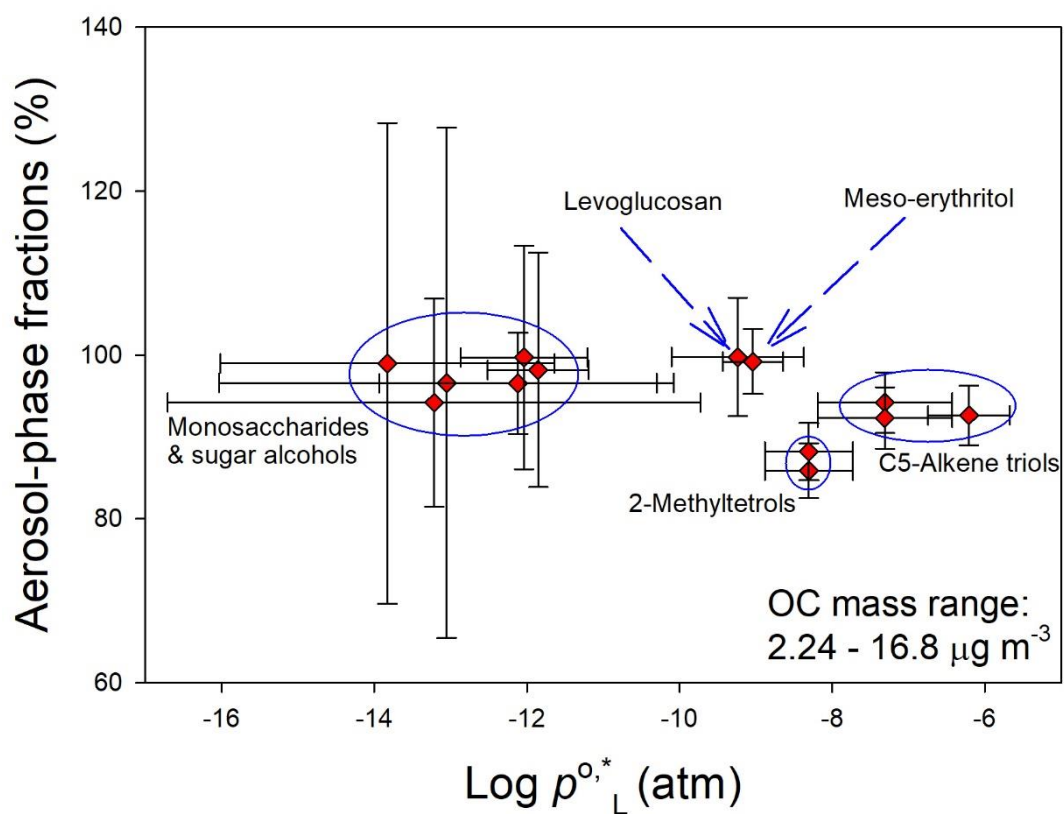


Figure 3. Average particle-phase fractions and $\log p^{0,*}_L$ of individual polyol tracers. Whiskers represent uncertainties of $F\%$ and one standard deviation of $\log p^{0,*}_L$ derived from different estimation tools.

Figure 4

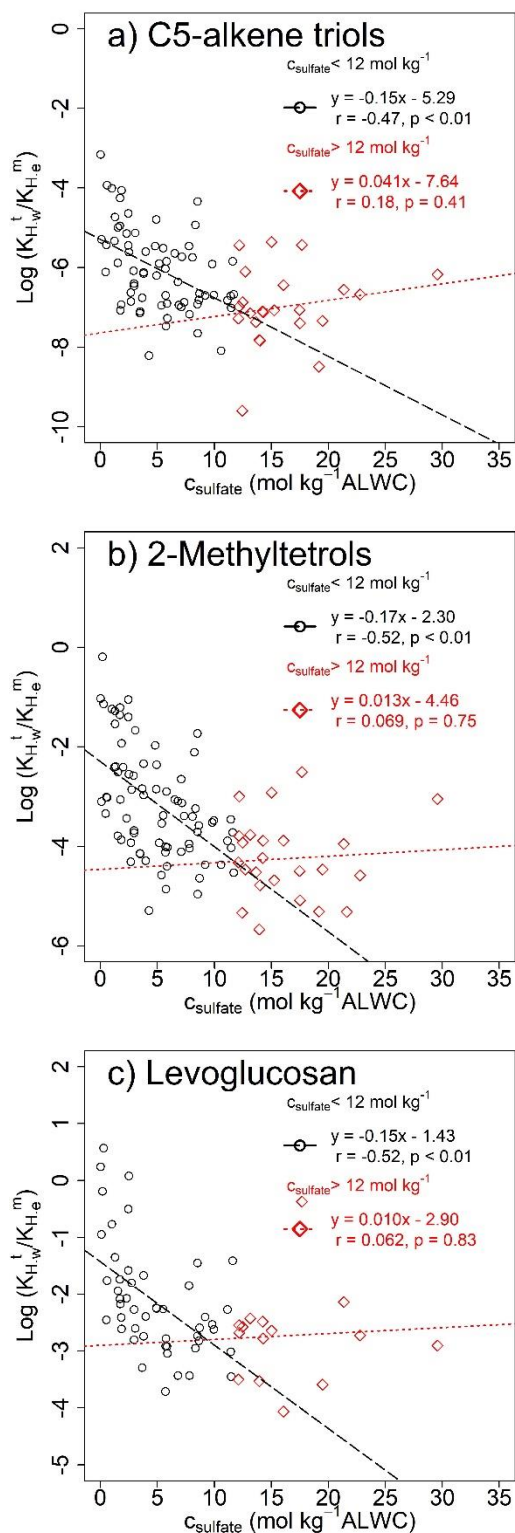


Figure 4. Modified Setschenow plots of $\log(K_{H,w}^t/K_{H,e}^m)$ versus c_{sulfate} for (a) C5-alkene triols, (b) 2-methyltetrols, and (c) levoglucosan.